ACS OMEGA

Open Access

http://pubs.acs.org/journal/acsodf

Article

Microfluidic Transfection System and Temperature Strongly Influence the Efficiency of Transient Transfection

Michaela Dehne, Simon Valentin Neidinger, Michael Stark, Antonia Camilla Adamo, Xenia Kraus, Nicolas Färber, Christoph Westerhausen, and Janina Bahnemann*

Cite This: *ACS Omega* 2024, 9, 21637−21646

Read Online

ACCESS | Metrics & More | Article Recommendations | Supporting Information

ABSTRACT: For the process of transient transfection (TTF), DNA is often transported into the cells using polyplexes. The polyplex uptake and the subsequent transient expression of the gene of interest are of great importance for a successful transfection. In this study, we investigated a 3D-printed microfluidic system designed to facilitate direct TTF for suspension of CHO−K1 cells. The results demonstrate that this system achieves significantly better results than the manual approach. Furthermore, the effect of both post-transfection incubation time (t) and temperature (T) on polyplex uptake was explored in light of the membrane phase transitions. Attention was paid to obtaining the highest possible transfection efficiency (TFE), viability (V), and viable cell concentration (VCC). Our results show that transfection output measured as product of VCC and TFE is optimal for t = 1 h at T = 22 °C. Moreover, post-transfection incubation at T = 22 °C with short periods of increased T at T = 40 °C were observed to further increase the output. Finally, we found that around T = 19 °C, the TFE increases strongly. This is the membrane phase transition T of CHO-K1 cells, and those results therefore suggest a correlation between membrane order and permeability (and in turn, TFE).

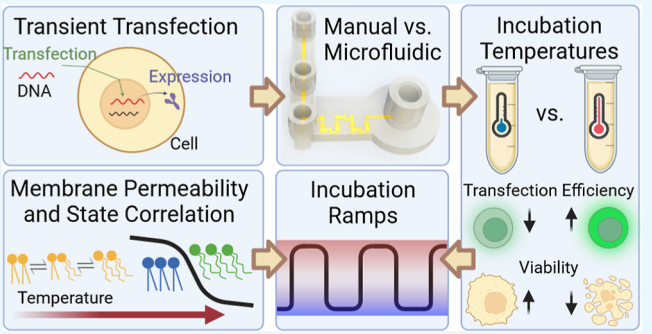

INTRODUCTION

Many modern biopharmaceuticals are produced via stable gene expression using stable transfected mammalian cells.[1] Unfortunately, stable transfection is a time-consuming process—which renders it far from ideal in many cases.[2] An intriguing potential alternative production mechanism is found in the process of transient gene expression (TGE). To achieve TGE, cells need to be transfected transiently, which is a much faster and significantly more flexible method that is already being used to produce biopharmaceuticals, albeit (to date) only in relatively small quantities.[2] The use of TGE with suspension mammalian cells, such as Chinese hamster ovary (CHO) or human embryonic kidney (HEK) cells, is of particular interest since suspension cell cultures are easily scalable and these cell types can produce biopharmaceuticals with human-like post-translational modifications.[3,4]

For transient transfection (TTF)—hereinafter referred to as transfection (TF)—different TF reagents can be utilized.[5] In this work, the commonly used TF reagent linear polyethylenimine (PEI) with 25 kDa was investigated.[6] PEI and DNA form a polyplex, which can then be readily taken up by the cells.[7] Although it is important to note that free PEI can actually have a cytotoxic effect.[7] For this reason, homogeneous mixing during TF is absolutely essential, so that the DNA and PEI form polyplexes quickly and PEI does not remain in a free state within the solution for very long.[5]

In seeking to solve that problem, we decided to explore whether a 3D-printed microfluidic system might be well-suited to ensure both quick and thorough mixing of these three components. For this reason, we integrated a micromixer (in particular a so-called HC mixer) into the microfluidic system in order to achieve homogeneous mixing of the three components at low flow rates with low shear stress for the cells.[8] 3D printing enables rapid prototyping, which means that the structures and parts being utilized can be quickly and individually adapted within a short time, in order to respond to results that are observed in the laboratory.[9]

In addition to the TF method, the time (t) of the following post-transfection incubation phase (during which the polyplexes are taken up by cells) is also of critical importance. In order to be taken up by cells, polyplexes must cross cell membranes via the vesicle-based methods of clathrin- or

Received: March 17, 2024
Revised: March 30, 2024
Accepted: April 4, 2024
Published: May 3, 2024

https://doi.org/10.1021/acsomega.4c02590
ACS Omega 2024, 9, 21637−21646

caveolae-mediated endocytosis.[7,10,11] Which endocytosis pathway is actually utilized depends on the size of the respective particle in question,[12] and these two uptake routes differ in both their speed and their transfection efficiency (TFE)—which is a measure of successful TF with subsequent TGE.[7,11] In adherent Henrietta Lacks (HeLa) cells and adenocarcinomic human alveolar basal epithelial (A549) cells, only caveolae-mediated uptake escapes the lysosomal destination and can thus become TF effective.[11,13] Unfortunately, there is a trade-off: this uptake pathway is significantly slower—which is why the post-transfection incubation period during which the polyplexes are being taken up is of crucial importance. In other experiments, it has already been shown that a longer post-transfection incubation time up to 4 h at 37 °C achieves the highest TFE with a polymer (PPI-123) and human doxorubicin-resistant breast adenocarcinoma cell line (MCF-7/ADR).[14] Similarly, an optimal post-transfection incubation time of 3 h at 37 °C was determined for adherent A549 cells with linear PEI of a molecular weight of M = 25 kDa.[11]

In addition, it has been intensively covered in the relevant literature that transport processes over the cell membrane can be mechanistically interpreted as a function of the phase state of the lipid membrane.[16] Accordingly, the distribution of the transport proteins to the different phases plays a decisive role.[16] The phase state of the lipids correlates with a number of observable parameters (including bending stiffness, permeability, membrane viscosity, as well as membrane thickness and area), and it can be influenced by a variety of factors (for example, by cholesterol levels, salt content, or the presence of an electric field).[17−22] Moreover, it has been shown that various transport processes for smaller molecules as well as nanoparticles depend on the phase state (or lipid order) of lipid and plasma membranes for both synthetic liposomes[22,23] and also biological membranes.[24] One of the most important factors influencing the phase state of lipid membranes is temperature (T).[17,25−27] While the phase transition of synthetic one or two component liposomes is limited to a T range of just a few degrees,[17] biological cells display a markedly broader phase transition range as well as a noticeable scattering of the phase state between individual cells, even under the same external conditions.[17,28]

For endocytotic uptake pathways, both membrane tension as well as the curvature of the membrane required for particle uptake must be taken into consideration.[29] It, therefore, stands to reason that there could also be a link between particle uptake rates and the thermodynamic state of the membrane when it comes to polyplex uptake. In fact, several publications have already suggested the existence of a link between the state of order of the cell membrane and certain endocytosis uptake pathways.[23,30−33] If this is the case, then for TF it could presumably be shown that a higher T (i.e., 37 °C vs 4 °C) has a higher uptake rate from polyplexes out of PPI-123 polymer and adherent MCF-7/ADR cells.[14]

The phase state of lipid membranes—especially the lipid order—can be determined using solvatochromic fluorescent dyes (such as Laurdan), which incorporates into the hydrophobic part of the lipid bilayer[15,17,29] and then emits light of different wavelengths depending on the dipolar relaxation of its environment.[34,35] Since the different phase states display different relaxation behaviors, this allows to infer the state of the membrane;[35] or, put in more concrete terms, after UV excitation, the emission maximum is located around λ = 440 nm in the ordered phase, and around λ = 490 nm in the disordered phase.[36]

Taking all of this into consideration, in this work, we set out to investigate whether improved mixing using a 3D-printed microfluidic TF system shows improved TFE and increased viability (V) when compared to the manual process. In addition, we also sought to focus on how best to optimize the biophysical factors of post-transfection incubation time (t) and temperature (T), in order to facilitate the uptake of polyplexes within this microfluidic system. Relatedly, we also investigated whether the membrane phase transition had any bearing on what we determined to be the optimal conditions for T.

EXPERIMENTAL METHODS

Microfluidic Design and Fabrication. The developed microfluidic system for direct TF contains 3 inlets—for the cells, DNA, and PEI, respectively—as well as an outlet for the transfected cells (Figure 1). The system is designed in such a way that first DNA and PEI solutions from two channels are combined in one, and then the cell suspension is added to this channel. The entire suspension is then passed through an integrated HC mixer, where all components are homogeneously mixed together in less than 1 s under low shear stress.[8] The integrated passive HC mixer operates according to the split-and-recombine mechanism. The volume flow is separated and mixed again, and this is repeated several times.[8]

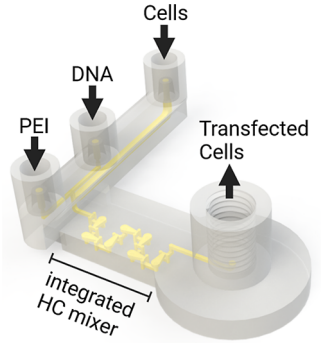

Figure 1. Microfluidic transfection system. Illustration of the 3D-printed microfluidic system with an integrated HC mixer.

The microfluidic system was designed with SolidWorks (Dassault Systems Deutschland GmbH, Stuttgart, Germany), and it was then 3D-printed by using a high-resolution MultiJet 3D printer (ProJet MJP 2500 Plus, 3D Systems, Rock Hill, SC, USA). VisiJet M2S-HT90 was used as the printing material and VisiJet M2 Sup as the heat-labile support material. The used printing material is a high-temperature-resistant biocompatible plastic (polyacrylate) that can be autoclaved for sterilization.[37]

After the printing process was complete, the printing plate was incubated for 10 min at −18 °C to remove the microfluidic system from the plate, and then it was transferred to a heat steam bath in an EasyClean unit (3D Systems, Rock Hill, SC, USA) for 45 min to remove the support material. The parts were then placed in a 65 °C paraffin oil bath (CarlRoth, Karlsruhe, Germany) for 30 min and rinsed several times with the hot oil in an ultrasonic bath (Elma Schmidbauer GmbH, Singen, Germany). After that, the parts were incubated in an ultrasonic bath (Bandelin electronic, Berlin, Germany) with detergent (1% (v/v) Fairy Ultra Plus, Procter and Gamble,

https://doi.org/10.1021/acsomega.4c02590
ACS Omega 2024, 9, 21637−21646

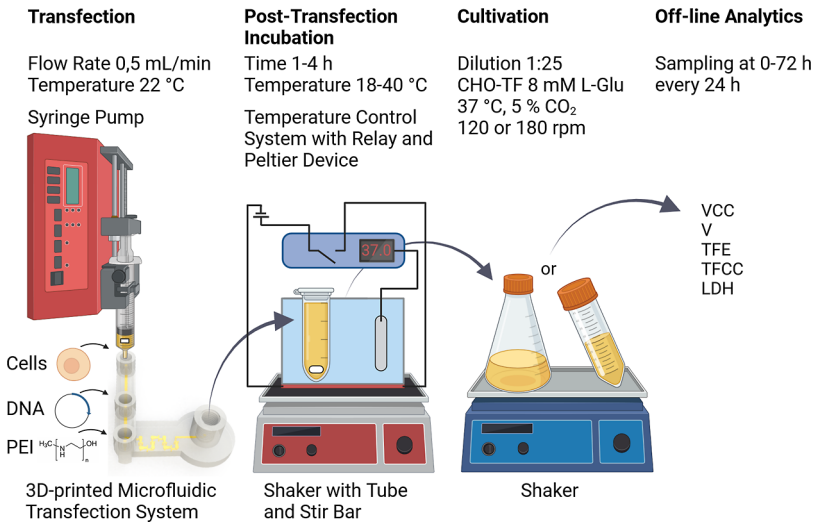

Figure 2. Schematic illustration of the individual steps from TF, post-transfection incubation, and cultivation to off-line analysis. During the TF step, the cells (mixed with a stir bar), DNA, and PEI were all pumped through the microfluidic TF system and into the incubation system. Afterward, the cells were stirred and incubated for a designated time at controlled and designated temperature. In the next step, the cells were diluted 1:25 with cell culture medium and then cultivated up to 72 h. Every 24 h the VCC, V, TFE, and LDH concentrations were measured (Created with Biorender.com).

CT, USA) for 30 min at 65 °C. This water-detergent mixture was flushed through the microfluidic channels and replaced until there was no more oil residue observed in the runoff. Afterward, the system was flushed with water (Arium Sartorius Stedim Biotech GmbH, Göttingen, Germany) until there was no detergent residue observed, either. Finally, the microfluidic system was connected with tubing and connectors and then sterilized via autoclaving for 30 min at 121 °C (Systec VX-150, Systec GmbH, Linden, Germany).

Cell Culture. For this study, a CHO-K1 cell line was used and cultivated in CHO-TF medium (Xell AG, Bielefeld, Germany), which was supplemented with 8 mM L-glutamine (Sigma-Aldrich Chemie GmbH, Steinheim, Germany) in a 5% CO_2 humidified atmosphere at 37 °C (Heracell vios 160i CO_2 incubator, Thermo Fisher Scientific Inc., Waltham, USA). Cells were grown at 120 or 180 rpm, with a cultivation volume of 25 or 12.5 mL in 100 mL shake flasks featuring baffles (ROTILABO, Carl Roth GmbH + Co. KG, Karlsruhe, Germany) with ventilation screw caps (DURAN with ePTFE membrane, Carl Roth GmbH + Co. KG, Karlsruhe, Germany), or in 50 mL bioreactor tubes (CELLSTAR, Greiner Bio-One GmbH, Frickenhausen, Germany) with a cultivation angle of 45° on an orbital shaker (CO_2 Resistant Shaker, Thermo Fisher Scientific Inc., Waltham, USA) with a diameter of 19 mm. The cells were inoculated with 0.3 × 10^6 cells/mL and split every 3−4 days.

Transient Transfection. The TF process was started, at the earliest, 3 passages after thawing and 24 h before TF the cells were diluted to 1.5 × 10^6 cells/mL. TF was performed using 25 kDa linear PEI (Polysciences, Inc., Warrington, USA) and an enhanced green fluorescent protein (eGFP) plasmid (pDSG-103-eGFP, 5828 bp, IBA Lifesciences GmbH, Göttingen, Germany), with the following final concentrations: cells 20 × 10^6 cells/mL; PEI 64 μg/mL, eGFP-plasmid 24 μg/mL. The cells were centrifuged for 5 min at 300*g* before being resuspended in the appropriate volume of 37 °C prewarmed CHO-TF (containing 8 mM L-glutamine) and then shaken for 30 min at 180 rpm in a bioreactor tube in the incubator.

For the TF process, syringes were loaded with the solutions of PEI, DNA (2 mL syringes), and cell suspension (20 mL syringe). The cell suspension was filled into a syringe together with a stir bar to ensure that thorough mixing of the cells was preserved. All syringes were placed into a custom-made holder on a syringe pump and connected to the microfluidic system (for a photo of the real setup, see Figure S1 in the Supporting Information). All solutions were pumped through the microfluidic transfection system using a syringe pump to produce an accurate mixing ratio via the integrated HC mixer.[8] The transfection was performed at a flow rate of 0.5 mL/min (syringe diameter 20.21 mm, resulting flow rate of 0.735 mL/min) with the following volumes of the prepared solutions: Cell suspension 9.6/1.36 mL; DNA and PEI each 2.2/0.32 mL (comparison manual vs microfluidic/temperature-dependent experiments). The controls were also injected using this method—but instead of PEI and DNA solutions, only the medium was dispersed into the system. The TF of the manual sample was performed by first adding the DNA, followed by the PEI, drop-by-drop, and while also simultaneously swirling the culture itself. Three replicates were created for each sample.

The post-transfection incubation phase was performed in airtight 15/2 mL (comparison manual vs microfluidic/temperature-dependent experiments) tubes or for experiments without oxygen limitations in 15 mL tubes with membrane cap and round-bottom (TPP Techno Plastic Products AG, Switzerland) under a biosafety cabinet at room temperature T = 22 °C (comparison transfection methods) or in the temperature control system at a certain temperature (temperature depending experiments). Cells were mixed by using small stir bars and a stirrer. After the post-transfection incubation period, cells were diluted 1:25 with prewarmed and gassed (37 °C and 5% CO_2) CHO-TF medium with 8 mM L-glutamine and cultivated analogously to standard cultivation (see section "Cell Culture"). The time after TF and post-transfection incubation phases started with the dilution in the cultivation phase. Within the cultivation phase, samples were taken at 0, 24, 48, and 72 h to determine viability (V), viable cell

https://doi.org/10.1021/acsomega.4c02590
ACS Omega 2024, 9, 21637−21646

concentration (VCC), transfection efficiency (TFE), and lactate dehydrogenase (LDH) concentration, and to determine the calculated transfected cell concentration (TFCC).

The TF process with the microfluidic system and the following steps are shown in Figure 2.

For the "time-dependent post-transfection incubation temperature profile" experiments, we used different "symmetric" and "asymmetric" T profiles. For the symmetric T profiles (Figure 3A), a baseline temperature (B) was used for

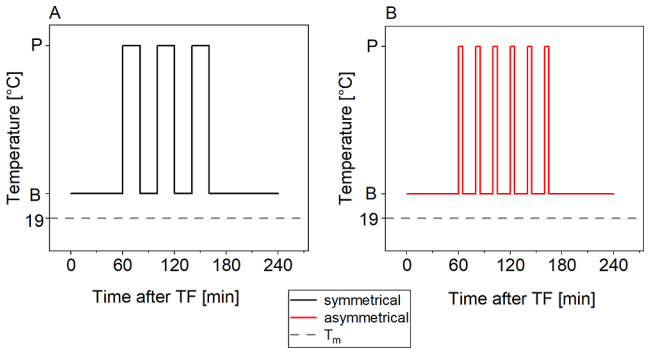

Figure 3. Presentation of time-dependent post-transfection incubation temperature profiles. Exemplary temperature profiles for symmetrical (A) and asymmetrical (B) post-transfection incubations.

the first hour of incubation. A second T (P) was then applied for 20 min, followed by a 20 min relaxation at the baseline temperature T. This sequence was repeated three times before incubation was resumed at the baseline temperature T until the four h incubation period was completed. The asymmetric (*asym*) T profile (Figure 3B) was also held for 60 min at $T = B$, followed by 5 min of $T = P$, followed by 15 min at $T = B$. These temperature variations were repeated 6 times. The remaining incubation time was completed at $T = B$. The following applies to the exemplary designation 22S40: 22 stands for the base temperature B = 22 °C, 40 for a peak temperature P = 40 °C, and S represents the sample (vs C for control). The time sequence of all T profiles can be found in Supporting Information Figure S2.

Off-Line Analytics. The VCC and V of the cells were analyzed using a trypan blue-assay-based Cedex cell counter or LUNA-II (Cedex HiRes, Roche Diagnostics GmbH, Mannheim, Germany, or Logos Biosystems, South Korea). To determine the TFE, 10,000 events were measured using a flow cytometer (BD Accuri C6, Becton Dickinson, NY, USA, or Cytoflex, Beckman Coulter, USA). A 488 nm OD1 filter was used in the flow cytometer for the experiments with different temperatures and temperature profiles.Out of the living population, the GFP-expressing cells were observed and counted under duplet discrimination. To prepare the cells for flow cytometry, they were centrifuged at 300 *g* for 5 min and then resuspended in phosphate-buffered saline (PBS). Subsequently, to calculate TFCC, the determined TFE was multiplied by the measured VCC. In addition, for the samples used to assess T optimization, LDH activity—which results from cell damage—was analyzed using a photometric Cedex Bio Analyzer (Roche Diagnostics GmbH, Mannheim, Germany).

Determination of the Temperature-Dependent Membrane Order. The generalized polarization (GP) measurements used to measure the membrane order as a function of T were carried out spectrometrically, using a custom-made setup that has previously been presented by Färber and Westerhausen.[17] In a 500 μL reaction tube, surrounded by an aluminum block, cell suspensions were analyzed optically during constant gentle mixing by a magnetic stirrer to avoid sedimentation. Over the range of T = −30 to 90 °C, the T was then regulated using a Peltier element with a corresponding Pt100 sensor placed in the cell suspension. The Laurdan-stained sample was excited at 360 nm by an ultraviolet LED with a UV bandpass, and the band-stop-filtered emitted light was passed to the spectrometer through an optical fiber (without focusing or any other optical components in the beam path). Across the entire T range, samples were scanned in T increments of ΔT = 1 K at a rate $\frac{dT}{dt}$ = 2 K/min. Protein denaturation above T = 40 °C may have an influence on the membrane order and fluorescence spectra of the first upscan; we therefore only evaluated the reversible results of the downscans from T = 90 °C to T = −30 °C.[17]

To prepare the samples, the cell suspension was brought up to the desired concentration of 20 × 10^6 cells/mL via centrifugation (5 min, 300*g*) and subsequent resuspension in medium, after using a semiautomated cell counter (LUNA-II, Logos Biosystems, South Korea). The samples were then stained using 1% Laurdan solved in dimethyl sulfoxide (DMSO) (stock concentration 1 mg/mL) and incubated for t = 2 h at T = 37 °C on a shaker at 120 rpm. After that, the samples were centrifuged once again, and then resuspended in the same manner as mentioned above, in order to minimize background fluorescence of unbound Laurdan. For determining the phase state of the membrane, the GP value was calculated based on the two intensity values (I) at wavelengths λ = 440 nm and λ = 490 nm using the relation $GP = \frac{(I_{440} - I_{490})}{(I_{440} + I_{490})}$.[17,36,38]

RESULTS AND DISCUSSION

In the following section, the order−disorder phase transition of the used CHO cells is first presented. Second, the transfection efficiency (TFE) is studied using conventional manual mixing of the components (cells, DNA, and PEI) and the presented microfluidic approach. Third, TF for various but constant post-transfection incubation T is shown. Finally, the trade-off between viability (V) and TFE is investigated and optimized by time-dependent post-transfection incubation temperature profiles. These results are discussed in light of membrane state-dependent permeability.

Phase Transition of CHO-K1 Cells. Figure 4 shows the generalized polarization GP as a function of T as the mean of three independently prepared samples of CHO-K1 cells. In addition, Figure 4 also shows the derivative of GP with respect to T. The resulting peak indicates the position and width of the T range with the strongest change in phase state and thus membrane order. Here, the transition T is about T_m = 19 °C − a comparable value as shown for other cell lines, as, e.g., HeLa cells.[17] Recently, it was shown for HeLa cells that the membrane order and the permeability of the plasma membrane correlate.[24] Thus, in the following sections, where we quantify transfection, we also discuss T effects against the background of the membrane phase transition of CHO cells.

Transfection Efficiency Employing a Manual and a Microfluidic Approach. For the first comparison of TF methods, the TFE, V, VCC (viable cell concentration), and

https://doi.org/10.1021/acsomega.4c02590
ACS Omega 2024, 9, 21637−21646

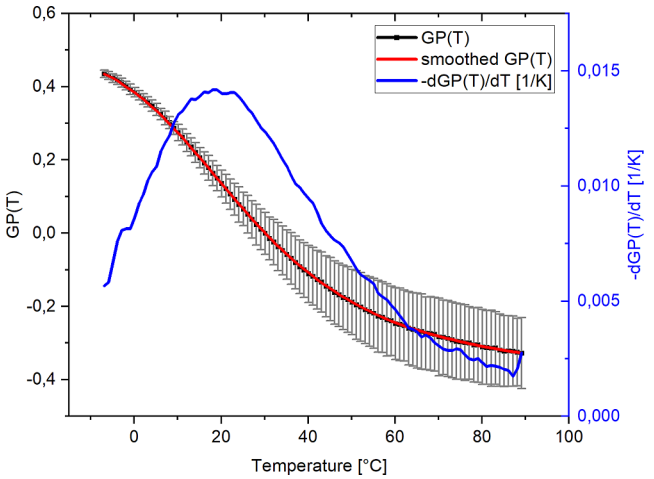

Figure 4. Temperature-dependent generalized polarization of CHO-K1 cells. Black squares: GP as a function of temperature for CHO cells (mean and standard deviation of $N = 3$ independent measurements). Red line: smoothed GP (T). Blue line: First derivative of the averaged GP (T) with respect to temperature. The data show that the membrane order is high at lower temperatures and changes to an increasingly disordered state with increasing temperature. The fastest change in order of the membrane is at a temperature of $T = 19$ °C (peak of the derivative of GP with respect to temperature).

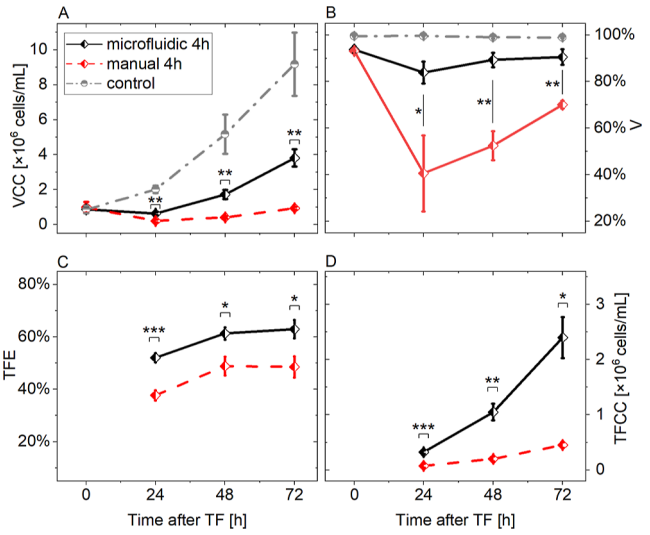

Figure 5. Results of microfluidic and manual TF. Control (gray), microfluidic (black), and manual (red). TF with 4 h post-transfection incubation time at 22 °C over 0−72 h. A: VCC, B: V, C: TFE, and D: TFCC. The symbols represent mean values of $N = 3$ experiments, while error bars represent the standard deviation. *, ** and *** represent P-values of <0,05, <0,01, and <0,001. The full data for the statistical analysis can be found in Supporting Information Table S1. The experiment clearly shows that the microfluidic approach achieves better results for all key parameters and ultimately in respect to TFCC.

TFCC (calculated transfected cell concentration) of the microfluidic and manual TF are determined under conditions that could be easily implemented with post-transfection incubation at room temperature ($T = 22$ °C). The microfluidic transfection was performed with the microfluidic transfection system, the manual transfection via pipetting, and the control was performed only with medium without DNA and PEI (see "Experimental Methods").

Figure 5 shows V, TFE, VCC, and the TFCC using both methods for up to 3 days after TF. Immediately following TF, no difference was observed in VCC (see Figure 5A) between the samples and the control (0.86−0.98 × 10^6 cells/mL). After 24 h, a decrease of VCC was seen in both the manual (0.20 × 10^6 cells/mL) and the microfluidic samples (0.62 × 10^6 cells/mL). Within 72 h, VCC increased most rapidly in the control (9.20 × 10^6 cells/mL), less in the microfluidic sample (3.81 × 10^6 cells/mL), and least of all within the manual sample (0.94 × 10^6 cells/mL).

By contrast, as shown in Figure 5B, V is already slightly reduced compared to the control immediately after TF using both methods. This is followed by a sharp V drop after 24 h to $V = 84\%$ (microfluidic) and $V = 41\%$ (manual). While the microfluidic transfected cells recover to $V = 91\%$ after 72 h, the manually transfected samples only reach $V = 70\%$.

The TFE is shown in Figure 5C. After just 24 h, there is a clear difference between the manually prepared (TFE = 38%) and microfluidically prepared (TFE = 52%) samples. By the final time point of 72 h, the TFE had risen to TFE = 49% (manual) and TFE = 63% (microfluidic), respectively.

The product TFCC out of TFE and VCC is shown in Figure 5D. 24 h after transfection, the microfluidic sample already reached a 4-fold TFCC compared to the manual sample (TFCC = 0.32 vs 0.08 × 10^6 cells/mL). This increases to 5.3 times in the course of cultivation after 72 h (TFCC = 2.4 vs 0.45 × 10^6 cells/mL).

Detailed data on TFE, V, VCC, and TFCC as functions of post-transfection incubations between $t = 1−4$ h can be found in the Supporting Information (Figure S3). In sum, almost all values (TFE, V, VCC, and TFCC) at post-transfection incubation times of $t = 1−4$ h are higher for the microfluidic samples than for the manual ones. Only the TFE with a post-transfection incubation time of 1 h for the microfluidic samples is lower than the manual sample with 1 h incubation time. In addition, only a minor influence on the post-transfection incubation time was observed for both of the TF methods.

The decrease in V and VCC after 24 h might be explained by the toxic effects of free-state PEI.[5,39,40] During TF, the cells come into contact with the PEI, and as a result, the V and VCC decrease. During cultivation, the cells begin to divide again, which is why V and VCC both increase. However, a significant difference was observed between the microfluidic and manual samples−so it can be assumed that the homogeneous mixing (see Experimental Methods "Microfluidic Design and Fabrication") in the microfluidic system can reduce the toxicity effect.

In summary, the microfluidic TF system achieves significantly better results than the manual method. In the following investigations, this method is applied to answer the question of whether the post-transfection incubation temperature and the phase state of the cell membrane play an important role in TF and polyplex uptake. For this purpose, it was examined at which post-transfection incubation temperature the transfection works best and how this correlates with the order of the cell membrane (compare Figure 4).

Transfection under Variation of the Post-Transfection Incubation Temperature. Here, we study the influence of various but constant post-transfection incubation (in the following only incubation) T ($T = 18$, 22, 28, 34, 37 and 40 °C), including the physiological temperature $T = 37$ °C

https://doi.org/10.1021/acsomega.4c02590
ACS Omega 2024, 9, 21637−21646

on TFE, V, VCC, TFCC, and LDH using microfluidic TF with a 4 h post-transfection incubation time (Figure 6). In addition, controls were also incubated over the whole T range at T = 18, 37, and 40 °C. The LDH data are shown in the Supporting Information (Figure S4).

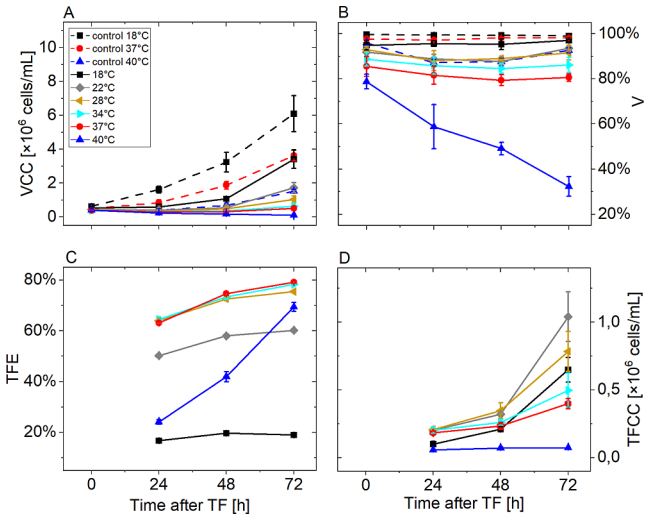

Figure 6. Results of TF with different post-transfection incubation temperatures. Microfluidic TF with a 4 h post-transfection incubation time at different temperatures over 0−72 h. A: VCC, B: V, C: TFE, and D: TFCC. The symbols represent mean values, while error bars represent the standard deviation.

The VCC (Figure 6A) shows that the cell concentrations of the controls are, in each case, above the values of the corresponding transfected samples. However, it can also be clearly seen that after 72 h, the controls exhibited markedly lower VCC at increased post-transfection incubation T. For the transfected samples after 72 h, the VCC was increasingly lower at higher T, with a particularly remarkable difference observed between the T = 18 and 22 °C samples (about a factor of 2 after 72 h). The TF with post-transfection incubation above T = 34 °C does not lead to a relevant increase in VCC within the first 72 h.

The V (Figure 6B) of all samples (T = 18−37 °C) and controls (T = 18, 37, or 40 °C) was notably higher (between 80 and 100%) throughout the whole cultivation time than that of the 40 °C sample at the beginning (which was initially 78% and dropped to 32% during cultivation after 72 h). Looking even more closely at the results after 72 h, the controls at T = 18 and 37 °C and the sample T = 18 °C have the highest V. In total, the V decreases in all samples and controls with increasing T. However, it should be noted that the control at T = 40 °C also has a V comparable to samples at T = 22 and 28 °C.

The LDH concentrations show a very similar picture (mirror image) as the viability data (see Supporting Information Figure S4). The LDH concentration increases with increasing temperature after 0 h in both controls and samples. For all controls and samples, except the T = 40 °C sample, the LDH concentration remains approximately constant or even decreases during cultivation. In the T = 40 °C sample, however, the values continue to increase during cultivation from 165 to 1226 nU/cell.

The TFE is shown in Figure 6C. For T = 18 °C during post-transfection incubation, the TFE is almost negligibly low. For a post-transfection incubation at T = 22 °C, already after 24 h TFE reaches values of about 50% and increases slightly over the next 2 days to TFE ≈ 60%. In the T range from T = 28 to 37 °C, all samples show a comparable value of TFE ≈ 63% and slightly increase over the whole cultivation time to TFE ≈ 75−79%. For T = 40 °C, TFE 24 h after transfection is about TFE ≈ 24% and increases steeply to TFE ≈ 69% after two further days of cultivation.

The TFCC for all samples at T = 18−37 °C increased clearly over the cultivation time (Figure 6D). For the sample T = 40 °C, the TFCC increases only slightly within 72 h (0.056−0.074 × 10^6 cells/mL). However, the increase in TFCC over the cultivation time diminished with increasing temperature; for example, sample T = 18 °C showed an increase of 6.5 times, whereas sample T = 40 °C showed only an increase of 1.3 times.

Since the results are most evident after 72 h, Figure 7 shows the results of VCC, V, TFE, and TFCC after 72 h depending

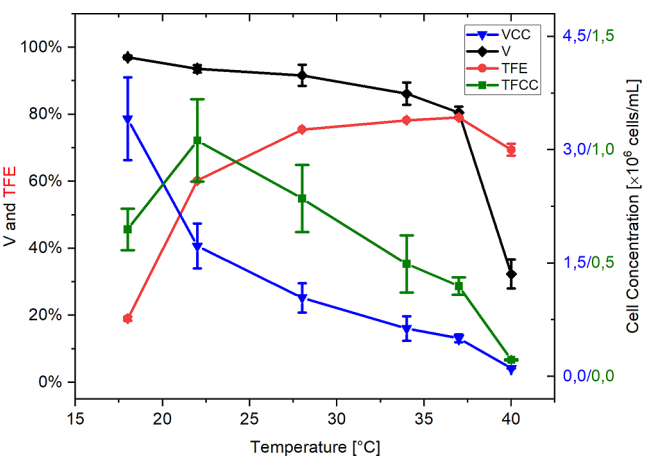

Figure 7. Results of transfection after 72 h as a function of the post-transfection incubation temperature. Results of microfluidic transfected cells with 4 h post-transfection incubation time at different temperatures. VCC (blue), V (black), TFE (red), and TFCC (green). The symbols represent mean values, while error bars represent the standard deviation.

on the post-transfection incubation T (the data after 24 and 48 h are shown in the Supporting Information Figures S5 and S6). The V and VCC as a function of T clearly show that these quantities diminish with the increasing T, whereas the TFE increases with rising T up to T = 37 °C and then decreases again at T = 40 °C. In the case of TFCC, an increase up to T = 22 °C and then a decrease up to T = 40 °C can be observed. Regarding TFCC, a local maximum is apparent around T = 22 °C, which is close to the phase transition of the CHO cells.

In summary, it can be stated that post-transfection incubation temperature T certainly exerted a considerable direct influence on the individual metrics outlined above. The TFE increased markedly with increasing T up to T = 37 °C, which suggests that the cells were better able to carry out the active endocytosis process at higher T. In addition, the samples but especially the controls demonstrated a decrease in VCC and V at higher T, including temperatures in the physiological range (T = 37 or 40 °C), which suggests not only that transfection at higher T has an influence on cells but also that the method of transfection exerts an additional influence. Due to the selected method, oxygen limitation may occur as no

https://doi.org/10.1021/acsomega.4c02590
ACS Omega 2024, 9, 21637−21646

oxygen or gas exchange is possible in the selected experimental setup. In addition, the CHO cells have a higher oxygen consumption at higher temperatures.[41] The observed effects could therefore also be due to the stress induced by oxygen limitation. For this reason, this series of experiments was repeated under identical conditions but using 15 mL cell culture reaction tubes with membrane lids as post-transfection incubation vessels. This setup allows for increased air volume within the vessel, facilitating gas exchange while preserving sterility. In the following, the results are presented (analogous to those depicted in Figure 7 of the previous experiment) without oxygen limitation (see Figure 8). Comprehensive

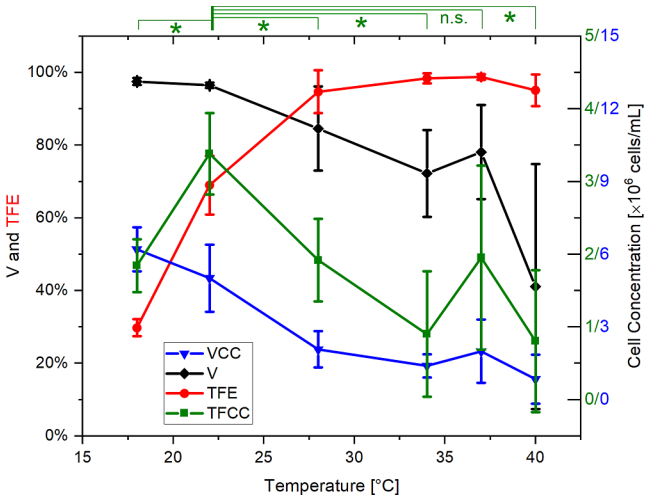

Figure 8. Results of transfection after 72 h as a function of the post-transfection incubation temperature without oxygen limitation. Results of microfluidic transfected cells with 4 h post-transfection incubation time at different temperatures. VCC (blue), V (black), TFE (red), and TFCC (green). $N = 3$. The symbols represent mean values, while error bars represent the standard deviation. The results of the TFCC for all samples were analyzed for significance in comparison to the sample at $T = 22$ °C. * represents a P-value of <0.05, n.s. indicates no significance (see Supporting Information Table S2).

experimental findings are shown in Figure S7. Furthermore, Supplementary Figures S8 and S9 (see Supporting Information) illustrate the variations in parameters TFE, V, VCC, and TFCC concerning temperature at 24 and 48 h intervals.

When comparing the results with potential and without oxygen limitation, it is evident that higher TFE can be achieved without oxygen limitation (maximum 79% vs 99%). In addition, higher VCC (max. 3.5 vs 6.20 × 10^6 cells/mL) and thus also higher TFCC (max. 0.47 vs 3.38 × 10^6 cells/mL) can be achieved without oxygen limitation. When considering TFCC, the trend with and without oxygen limitation is very similar—an optimum at $T = 22$ °C can be observed in each case. Additionally, a local optimum can be determined at $T = 37$ °C in the samples without oxygen limitation. However, the local optimum could only be determined for one of three replicates. However, the V from the sample at $T = 28$–40 °C without oxygen limitation is lower than that in the samples with potential oxygen limitation. This can be explained by the increased uptake of polyplexes, which is associated with increased TFE and TFCC and lower V. In summary, it can be concluded that potential oxygen limitation only leads to a reduced uptake of polyplexes, resulting in decreased TFE and TFCC, and relatively higher V. However, it does not fundamentally alter the observed results with a potential oxygen limitation. Furthermore, we measured the pH value before (pH = 7.45) and after the transfection gassed with 5% CO_2 (pH = 7.26) and not gassed (pH = 7.12) (post-transfection incubation temperature 37 °C). Since only very small differences can be observed in the pH value, this should have no influence on the viability or growth of the cells.

Overall, it can be noted in both cases that the TFE increases with temperature up to $T = 37$ °C. This improved uptake of the polyplexes, and the increased TFE at $T = 37$ °C, has previously been described in the literature.[14] However, for production of recombinant proteins/biopharmaceuticals, this work shows that not only a TFE but also a high VCC should be achieved. Therefore, in order to determine the optimal post-transfection incubation T, the VCC, and the TFE must be included, which in our case was expressed by the TFCC. In this investigation, the TFCC showed a local maximum around $T = 22$ °C. Interestingly, this is in the region of the main phase transition of the CHO cells—which further suggests that lipid membrane properties (i.e., those that change most strongly in the transition regime) actually do contribute to the transfection process. To account for the mismatch between optimal T for permeabilization/polyplex uptake and V/VCC, in the following section, we also introduce time-dependent T profiles during post-transfection incubation to further increase TFCC.

Post-Transfection Incubation at Time-Dependent Temperature Profiles. Based on the results shown above, the question now naturally arises as to whether there is a possibility of combining the advantages of the different T to achieve both a high VCC and a high TFE, which results in an even higher TFCC. For example, brief temperature variations could potentially increase membrane permeability, thereby also increasing the uptake of polyplexes. For this purpose, a further experiment was conducted to test the effect of time-varying post-transfection incubation T.

Two different T profiles entitled "symmetric" and "asymmetric" where investigated. For both temperature profiles, a baseline temperature $T = B$ was maintained and switched to a second peak temperature $T = P$. For the symmetric profiles, this was done at equal time intervals for the asymmetric profiles with longer dwell time at B and only short switches to P as described above in detail (see Figure 3). The idea of the asymmetric T profile compared to the symmetric was to see if only a short heat shock can improve the uptake from the polyplexes while at the same time, the viability is not affected much.

In Figure 9, the results of VCC, V, TFE, and TFCC of these applied profiles (labeled as BSP for transfected samples and BCP for controls) are shown. The data for LDH are also shown in Supporting Information Figure S10.

As in the previous experiments, it can be clearly seen from these results that the controls exhibited both a higher VCC and a higher V over the entire period of cultivation when compared with all investigated samples ($9A + B$). The viability results are also consistent with LDH measurements in these assays (see Supporting Information Figure S10). However, there was also a clear observable difference in VCC between the controls after 72 h: The control 22C40 had the highest VCC, followed by the 37C22 and 22C40 asym and then again followed by the 40C22 and 37C40 with notably lower VCC. From these results, it can indeed be concluded that the different T shifts

https://doi.org/10.1021/acsomega.4c02590
ACS Omega 2024, 9, 21637−21646

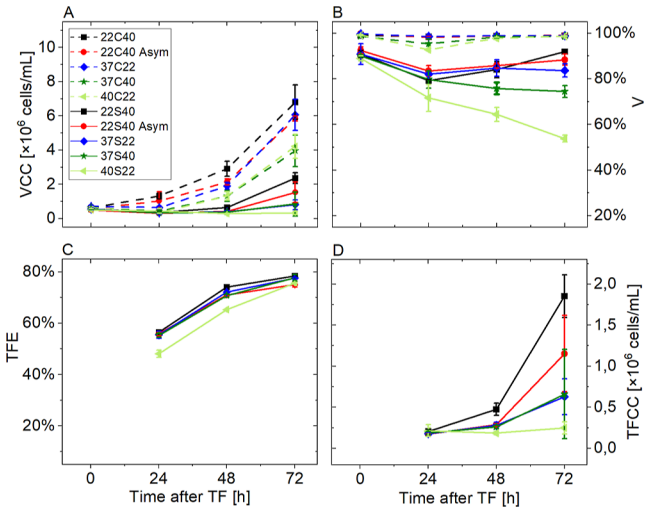

Figure 9. Results of the TF with different temperature profiles. Microfluidic transfected cells with a 4 h post-transfection incubation time with different temperature profiles. (A) VCC; (B) V; (C) TFE; (D) TFCC. The symbols represent mean values, while error bars represent the standard deviation.

alone affected the growth of the cells. This should be taken into consideration when discussing the samples.

In the samples, a clear difference in the VCC and V became evident after 72 h (Figure 9A+B). The samples showed both an increase in VCC and V, along the order 40S22, 37S40/37S22, 22S40 asym, and 22S40. With the TFE (Figure 9C), however, all samples had a TFE ≈ 55% after 24 h. Only the 40S22 had a lower value, with a TFE of ≈ 48%. All TFE values increased in the course of cultivation, especially that of the 40S22 sample so that after 72 h, all samples were at a TFE ≈ 75%. The TFCC (Figure 9D) is comparable with TFCC ≈ 0.22 × 10^6 cells/mL for all samples after 24 h. During the course of cultivation, TFCC increases differently within all samples resulting in the following after 72 h: 22S40 had the highest TFCC of 1.85 × 10^6 cells/mL, followed by 22S40 asym (1.15 × 10^6 cells/mL), 37S22 and 37S40 (0.66 × 10^6 cells/mL), and finally 40S22 (0.25 × 10^6 cells/mL). Overall, an improved TF can thus be observed in terms of TFCC at temperature profiles of 22S40 and 22S40 asym. Considering both samples, 22S40 showed a higher TFCC, from which it can safely be assumed that longer times at higher temperature (3 × 20 min vs 6 × 5 min) led to a further improved uptake of the polyplexes.

Comparison of sample 22S40 with the 22 °C cell sample from the previous experiment (with potential oxygen limitation) shows that the short-term temperature increases in the middle part of the post-transfection incubation period can clearly increase the TFE (from 60 to 78% after 72 h) without simultaneously inducing major long-term losses in cell viability (times over 48 h). Accordingly, such a T profile could actually improve the success of TF compared to TF at a fixed T, by combining the respective advantages of post-transfection incubation at different T. Here, this variation led to an increase of TFCC of ΔTFCC = +78%, as compared to the baseline post-transfection incubation T.

CONCLUSIONS

The uptake of polyplexes is critical within TF—, which is why the type of TF used, as well as the t and T parameters of the post-transfection incubation phase (during which the polyplexes are taken up), are all factors of great importance that should be carefully evaluated and considered. In addition to assessing TFE, we also recognized the significance of key parameters such as V and VCC, thus identifying TFCC (TFE × VCC) as an essential factor to consider. Within the scope of this work, it is shown that the microfluidic system developed for TF yields significantly better results in terms of VCC, V, TFE, and TFCC than a manual process.

We further investigated various constant incubation temperatures T and nonconstant temperature profiles $T(t)$ during the post-transfection incubation phase. Regarding the post-transfection incubation at constant T, our data demonstrate an optimum of TFCC at T = 22 °C. Moreover, our findings revealed that potential oxygen limitation diminishes VCC, TFE, and consequently, TFCC, while also enhancing V due to decreased polyplex uptake. Nonetheless, the presence of oxygen does not alter the correlation between the post-transfection incubation temperature and the TFCC optimum. Employing additional short phases of increased T (3 times T = 40 °C for 20 min) during the post-transfection incubation phase, we were able to increase TFCC even further (by ΔTFCC = +78%) as compared to the treatment at T = 22 °C (with potential oxygen limitation). Interestingly, this T optimum is close to the determined center temperature of the membrane order phase transition T_m of the CHO cells. This could be an indication that, particularly near the phase transition region, the nonlinearities in mechanical membrane properties have an impact on transport processes (such as endocytosis in the TF). This observation opens up fascinating new directions for investigations at the interdisciplinary interface between biophysics, cell culture technology, and biomedicine, for example, to improve drug-delivery approaches by controlling membrane permeability or to optimize transfection processes and the production of pharmaceutical products.

ASSOCIATED CONTENT

Supporting Information

The Supporting Information is available free of charge at https://pubs.acs.org/doi/10.1021/acsomega.4c02590.

Photo from the microfluidic transfection system, the temperature profiles, results of the comparison of microfluidic and manual TF at different post-transfection incubation times, and the LDH values of the measurements at constant (with potential and without oxygen limitation) and variable T (PDF)

AUTHOR INFORMATION

Corresponding Author

Janina Bahnemann − *Chair Technical Biology, Institute of Physics and Centre for Advanced Analytics and Predictive Sciences (CAAPS), University of Augsburg, Augsburg 86159, Germany;* orcid.org/0000-0002-7008-1673; Phone: +49 821-598 3308; Email: janina.bahnemann@uni-a.de

Authors

Michaela Dehne − *Institute of Technical Chemistry, Leibniz University Hannover, Hannover 30167, Germany; Chair Technical Biology, Institute of Physics, University of Augsburg, Augsburg 86159, Germany;* orcid.org/0009-0001-6015-1084

https://doi.org/10.1021/acsomega.4c02590
ACS Omega 2024, 9, 21637−21646

Simon Valentin Neidinger − *Physiology, Faculty of Medicine, Institute of Theoretical Medicine, University of Augsburg, Augsburg 86159, Germany;* orcid.org/0009-0004-5115-2693
Michael Stark − *Physiology, Faculty of Medicine, Institute of Theoretical Medicine, University of Augsburg, Augsburg 86159, Germany;* orcid.org/0009-0000-8600-8780
Antonia Camilla Adamo − *Physiology, Faculty of Medicine, Institute of Theoretical Medicine, University of Augsburg, Augsburg 86159, Germany;* orcid.org/0009-0002-1940-6169
Xenia Kraus − *Chair Technical Biology, Institute of Physics, University of Augsburg, Augsburg 86159, Germany;* orcid.org/0000-0002-1186-5443
Nicolas Färber − *Physiology, Faculty of Medicine, Institute of Theoretical Medicine, University of Augsburg, Augsburg 86159, Germany;* orcid.org/0000-0001-5070-0943
Christoph Westerhausen − *Physiology, Faculty of Medicine, Institute of Theoretical Medicine, Centre for Advanced Analytics and Predictive Sciences (CAAPS), and Institute of Physics, University of Augsburg, Augsburg 86159, Germany;* orcid.org/0000-0001-7103-7060

Complete contact information is available at: https://pubs.acs.org/10.1021/acsomega.4c02590

Author Contributions

The manuscript was written through contributions of all authors. All authors have given approval to the final version of the manuscript.

Notes

The authors declare no competing financial interest.

■ ACKNOWLEDGMENTS

The author J.B. acknowledges the financial support of the German Research Foundation (DFG) via the Emmy Noether Programme (346772917). M.D. and N.F. are supported by the Add-on Fellowship of the Joachim Herz Foundation. S.N. is supported by the Hanns-Seidel-Stiftung. C.W. would like to thank for support of the Center for NanoScience (CeNS) and the German Research Foundation (DFG) via the grant INST 94/135-1 FUGG. Moreover, J.B. and C.W. would like to acknowledge support by the transfer project WiR of the University of Augsburg and support by the program "Forschungspotenziale fördern" of the University of Augsburg Moreover, the authors thank Achim Wixforth for fruitful discussions.

■ ABBREVIATIONS

A549, adenocarcinomic human alveolar basal epithelial; asym, asymmetric; B, baseline temperature; BCP, control incubated at B with shifts to the P; BSP, sample incubated at B with shifts to P; CHO, Chinese hamster ovary; DMSO, dimethyl sulfoxide; eGFP, enhanced green fluorescent protein; GP, generalized polarization; HEK, human embryonic kidney; HeLa, Henrietta Lacks; LDH, lactate dehydrogenase; ma, manual; MCF-7/ADR, human doxorubicin-resistant breast adenocarcinoma cell line; mi, microfluidic; P: PBS phosphat-buffered saline, second temperature; PEI: sym symmetric, polyethylenimine; *T*, temperature; *t*, time; TF, transfection; TTF, transient transfection; TFCC, calculated transfected cell concentration; TFE, transfection efficiency; TGE, transient gene expression; V, viability; VCC, viable cell concentration

■ REFERENCES

(1) Kesik-Brodacka, M. Progress in biopharmaceutical development. *Biotechnol. Appl. Biochem.* **2018**, *65*, 306−322.
(2) Bandaranayake, A. D.; Almo, S. C. Recent advances in mammalian protein production. *FEBS Lett.* **2014**, *588*, 253−260.
(3) Dumont, J.; Euwart, D.; Mei, B.; Estes, S.; Kshirsagar, R. Human cell lines for biopharmaceutical manufacturing: history, status, and future perspectives. *Crit. Rev. Biotechnol.* **2016**, *36*, 1110−1122.
(4) Kim, T. K.; Eberwine, J. H. Mammalian cell transfection: the present and the future. *Anal. Bioanal. Chem.* **2010**, *397*, 3173−3178.
(5) Gutiérrez-Granados, S.; Cervera, L.; Kamen, A. A.; Gòdia, F. Advancements in mammalian cell transient gene expression (TGE) technology for accelerated production of biologics. *Crit. Rev. Biotechnol.* **2018**, *38* (6), 918−940.
(6) Boussif, O.; Lezoualc'h, F.; Zanta, M. A.; Mergny, M. D.; Scherman, D.; Demeneix, B.; Behr, J. P. A versatile vector for gene and oligonucleotide transfer into cells in culture and in vivo: polyethylenimine. *Proc. Natl. Acad. Sci. U.S.A.* **1995**, *92*, 7297−7301.
(7) Pandey, A. P.; Sawant, K. K. Polyethylenimine: A versatile, multifunctional non-viral vector for nucleic acid delivery. *Mater. Sci. Eng. C* **2016**, *68*, 904−918.
(8) Enders, A.; Siller, I. G.; Urmann, K.; Hoffmann, M. R.; Bahnemann, J. 3D Printed Microfluidic Mixers—A Comparative Study on Mixing Unit Performances. *Small* **2019**, *15*, No. e1804326.
(9) Au, A. K.; Huynh, W.; Horowitz, L. F.; Folch, A. 3D-Printed Microfluidics. *Angew. Chem. Int. Ed.* **2016**, *55*, 3862−3881.
(10) Amyere, M.; Mettlen, M.; van der Smissen, P.; Platek, A.; Payrastre, B.; Veithen, A.; Courtoy, P. J. Origin, originality, functions, subversions and molecular signalling of macropinocytosis. *Int. J. Med. Microbiol.* **2001**, *291*, 487−494.
(11) Rejman, J.; Bragonzi, A.; Conese, M. Role of clathrin- and caveolae-mediated endocytosis in gene transfer mediated by lipo- and polyplexes. *Mol. Ther.* **2005**, *12*, 468−474.
(12) Rejman, J.; Oberle, V.; Zuhorn, I. S.; Hoekstra, D. Size-dependent internalization of particles via the pathways of clathrin- and caveolae-mediated endocytosis. *Biochem. J.* **2004**, *377*, 159−169.
(13) Rejman, J.; Conese, M.; Hoekstra, D. Gene transfer by means of lipo- and polyplexes: role of clathrin and caveolae-mediated endocytosis. *J. Liposome Res.* **2006**, *16*, 237−247.
(14) Gu, J.; Hao, J.; Fang, X.; Sha, X. Factors influencing the transfection efficiency and cellular uptake mechanisms of Pluronic P123-modified polypropyleneimine/pDNA polyplexes in multidrug resistant breast cancer cells. *Colloids Surf. B Biointerfaces* **2016**, *140*, 83−93.
(15) Jurkiewicz, P.; Olzyńska, A.; Langner, M.; Hof, M. Headgroup hydration and mobility of DOTAP/DOPC bilayers: a fluorescence solvent relaxation study. *Langmuir : the ACS journal of surfaces and colloids* **2006**, *22*, 8741−8749.
(16) Thilo, L.; Träuble, H.; Overath, P. Mechanistic interpretation of the influence of lipid phase transitions on transport functions. *Biochemistry* **1977**, *16* (7), 1283−1290.
(17) Färber, N.; Westerhausen, C. Broad lipid phase transitions in mammalian cell membranes measured by Laurdan fluorescence spectroscopy. *Biochim. Biophys. Acta, Biomembr.* **2022**, *1864* (1), 183794.
(18) Heimburg, T.; Jackson, A. D. On soliton propagation in biomembranes and nerves. *Proc. Natl. Acad. Sci. U.S.A.* **2005**, *102*, 9790−9795.
(19) Steinkühler, J.; Sezgin, E.; Urbančič, I.; Eggeling, C.; Dimova, R. Mechanical properties of plasma membrane vesicles correlate with lipid order, viscosity and cell density. *Commun. Biol.* **2019**, *2*, 337.
(20) Heimburg, T. The capacitance and electromechanical coupling of lipid membranes close to transitions: the effect of electrostriction. *Biophys. J.* **2012**, *103*, 918−929.
(21) Böckmann, R. A.; Hac, A.; Heimburg, T.; Grubmüller, H. Effect of sodium chloride on a lipid bilayer. *Biophys. J.* **2003**, *85* (3), 1647−1655.
(22) Blicher, A.; Wodzinska, K.; Fidorra, M.; Winterhalter, M.; Heimburg, T. The temperature dependence of lipid membrane

permeability, its quantized nature, and the influence of anesthetics. *Biophys. J.* **2009**, *96*, 4581−4591.
(23) Strobl, F. G.; Seitz, F.; Westerhausen, C.; Reller, A.; Torrano, A. A.; Bräuchle, C.; Wixforth, A.; Schneider, M. F. Intake of silica nanoparticles by giant lipid vesicles: influence of particle size and thermodynamic membrane state. *Beilstein J. Nanotechnol.* **2014**, *5*, 2468−2478.
(24) Färber, N.; Reitler, J.; Schäfer, J.; Westerhausen, C. Transport Across Cell Membranes is Modulated by Lipid Order. *Adv. Biol.* **2023**, *6*, No. e2200282.
(25) Lee, A. G. Lipid phase transitions and phase diagrams. I. Lipid phase transitions. *Biochim. Biophys. Acta* **1977**, *472*, 237−281.
(26) Mabrey, S.; Sturtevant, J. M. Investigation of phase transitions of lipids and lipid mixtures by sensitivity differential scanning calorimetry. *Proc. Natl. Acad. Sci. U.S.A.* **1976**, *73*, 3862−3866.
(27) Overath, P.; Träuble, H. Phase transitions in cells, membranes, and lipids of Escherichia coli. Detection by fluorescent probes, light scattering, and dilatometry. *Biochemistry* **1973**, *12* (14), 2625−2634.
(28) Färber, N.; Reitler, J.; Schäfer, J.; Westerhausen, C. Membrane transport in cell ensembles is modulated by the membrane state. 2022, https://assets.researchsquare.com/files/rs-1297077/v1_covered.pdf?c=1643914791 (accessed Feb 8, 2023).
(29) Zhang, S.; Gao, H.; Bao, G. Physical Principles of Nanoparticle Cellular Endocytosis. *ACS Nano* **2015**, *9*, 8655−8671.
(30) Mamdouh, Z.; Giocondi, M. C.; Laprade, R.; Le Grimellec, C. Temperature dependence of endocytosis in renal epithelial cells in culture. *Biochim. Biophys. Acta* **1996**, *1282*, 171−173.
(31) Wolkers, W. F.; Looper, S. A.; Fontanilla, R. A.; Tsvetkova, N. M.; Tablin, F.; Crowe, J. H. Temperature dependence of fluid phase endocytosis coincides with membrane properties of pig platelets. *Biochim. Biophys. Acta* **2003**, *1612*, 154−163.
(32) Hilgemann, D. W.; Lin, M.-J.; Fine, M.; Deisl, C. On the existence of endocytosis driven by membrane phase separations. *Biochim. Biophys. Acta, Biomembr.* **2020**, *1862*, 183007.
(33) Fine, M.; Llaguno, M. C.; Lariccia, V.; Lin, M.-J.; Yaradanakul, A.; Hilgemann, D. W. Massive endocytosis driven by lipidic forces originating in the outer plasmalemmal monolayer: a new approach to membrane recycling and lipid domains. *J. Gen. Physiol.* **2011**, *137*, 137−154.
(34) Parasassi, T.; Conti, F.; Gratton, E. Time-resolved fluorescence emission spectra of Laurdan in phospholipid vesicles by multi-frequency phase and modulation fluorometry. *Cell. Mol. Biol.* **1986**, *32/1*, 103−108.
(35) Parasassi, T.; Gratton, E. Packing of phospholipid vesicles studied by oxygen quenching of Laurdan fluorescence. *J. Fluoresc.* **1992**, *2*, 167−174.
(36) Parasassi, T.; de Stasio, G.; Ravagnan, G.; Rusch, R. M.; Gratton, E. Quantitation of lipid phases in phospholipid vesicles by the generalized polarization of Laurdan fluorescence. *Biophys. J.* **1991**, *60* (1), 179−189.
(37) 3D Systems. VisiJet M2S-HT90 (MJP) | 3D Systems. 2019, https://de.3dsystems.com/materials/visijet-m2s-ht90-mjp (accessed June 22, 2023).
(38) Parasassi, T.; de Stasio, G.; d'Ubaldo, A.; Gratton, E. Phase fluctuation in phospholipid membranes revealed by Laurdan fluorescence. *Biophys. J.* **1990**, *57/6*, 1179−1186.
(39) Huh, S.-H.; Do, H.-J.; Lim, H.-Y.; Kim, D.-K.; Choi, S.-J.; Song, H.; Kim, N.-H.; Park, J.-K.; Chang, W.-K.; Chung, H.-M.; Kim, J.-H. Optimization of 25 kDa linear polyethylenimine for efficient gene delivery. *Biologicals* **2007**, *35*, 165−171.
(40) Godbey, W. T.; Wu, K. K.; Hirasaki, G. J.; Mikos, A. G. Improved packing of poly(ethylenimine)/DNA complexes increases transfection efficiency. *Gene Ther.* **1999**, *6*, 1380−1388.
(41) Jorjani, P.; Ozturk, S. S. Effects of cell density and temperature on oxygen consumption rate for different mammalian cell lines. *Biotechnol. Bioeng.* **1999**, *64*, 349−356.

https://doi.org/10.1021/acsomega.4c02590
ACS Omega 2024, 9, 21637−21646